Heliyon 10 (2024) e27359

Contents lists available at ScienceDirect

Heliyon

journal homepage: www.cell.com/heliyon

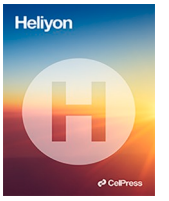

Research article

Tunable structure of TiO_2 deposited by DC magnetron sputtering to adsorb Cr (VI) and Fe (III) from water

F.A. Hernández-Rodríguez [a], R. Garza-Hernández [b], M.R. Alfaro-Cruz [a,c,*], Leticia M. Torres-Martínez [a,d]

[a] Universidad Autónoma de Nuevo León, Facultad de Ingeniería Civil, Departamento de Ecomateriales y Energía, Av. Universidad S/N Ciudad Universitaria, San Nicolás de los Garza, Nuevo León, C.P. 66455, Mexico
[b] Centro de Investigaciones en Óptica, A.C., Loma del Bosque 115, Col. Lomas del Campestre León, Guanajuato, C.P. 37150, Mexico
[c] CONAHCYT-Universidad Autónoma de Nuevo León, Facultad de Ingeniería Civil, Departamento de Ecomateriales y Energía, Ciudad Universitaria, San Nicolás de los Garza, Nuevo León, C.P. 66455, Mexico
[d] Centro de Investigación en Materiales Avanzados, S. C. (CIMAV), Miguel de Cervantes No. 120, Complejo Industrial Chihuahua, Chih., CP, 31136, Mexico

A B S T R A C T

TiO_2 thin films with mixtures of the anatase, rutile, and brookite phases were deposited on glass substrates via magnetron sputtering. Based on XRD and Raman results, the TiO_2-0.47 and TiO_2-3.47 films principally contained the brookite phase, while the TiO_2-1.27 and TiO_2-2.13 films were primarily anatase. The capacities of the TiO_2 films to adsorb heavy metals were tested with Cr(VI) and Fe(III) solutions, and the maximum Cr(VI) and Fe(III) adsorption capacities were realized with the TiO_2-0.47 film (334.5 mg/g) and TiO_2-3.47 film (271.3 mg/g), respectively. SEM–EDS results revealed the presence of Cr and Fe on the surfaces of the films, thus corroborating the ability of the TiO_2 films to adsorb and remove heavy metals. They are strong candidates for use in wastewater treatment plants.

1. Introduction

TiO_2 is the most promising photocatalytic semiconductor due to its excellent physicochemical properties, high chemical stability, nontoxicity, long-term photoactivity, high stability under UV irradiation, etc. [1–4]. As a photocatalyst, TiO_2 has mainly been used in dye degradation, and it was reported to degrade up to 92–95% of the methylene blue (MB) and 96% of rhodamine B (RhB) in solution [5,6]. High photocatalytic efficiency resulted from irradiation of TiO_2, during which it generated electron-hole pairs; the electrons had high reduction potentials and the holes at the semiconductor surface had high oxidation potentials, which enabled the breakdown of organic molecules by ·OH radicals [4]. In addition, TiO_2 has been used in other photocatalytic reactions, such as hydrogen generation and CO_2 reduction, which have gradually become more important due to the high efficiency of TiO_2 [7,8]. Based on these photocatalytic applications in which TiO_2 can be used, it is an excellent option for water remediation via adsorption of heavy metals. In an adsorption process, the metallic species present in an aqueous solution are adsorbed on the surface of a solid, and adsorption occurs through electrostatic charges [9]. Since heavy metals have high affinities for hydroxyl species (OH^-), TiO_2 is used for adsorption of heavy metals; as noted above, TiO_2 generates abundant OH^- species, which increases the probability of adsorbing the metals and the efficiencies of photocatalytic reactions used for water remediation [9,10]. In this sense, TiO_2 adsorbs different heavy metals, such as Pb^{2+}, Cu^{2+}, Cd^{2+}, Ni^{2+}, and Cr^{6+} [11–20]. However, most of the reported studies have used TiO_2 as a powder, which is a problem

* Corresponding author. Universidad Autónoma de Nuevo León, Facultad de Ingeniería Civil, Departamento de Ecomateriales y Energía, Av. Universidad S/N Ciudad Universitaria, San Nicolás de los Garza, Nuevo León, C.P. 66455, Mexico
E-mail addresses: malfaroc@uanl.edu.mx, mralfaro@conahcyt.mx (M.R. Alfaro-Cruz).

https://doi.org/10.1016/j.heliyon.2024.e27359
Received 27 September 2023; Received in revised form 27 February 2024; Accepted 28 February 2024
Available online 5 March 2024

when the photocatalyst is to be recovered; alternatively, other semiconductors or organic compounds can be added with TiO_2 to increase the adsorption efficiency, as shown in Table S1.

In contrast, TiO_2 is a very attractive semiconductor due to the three crystalline phases anatase, rutile, and brookite, which influence the efficiency of TiO_2 in each photocatalytic process in different ways. Among the three crystalline phases of TiO_2, anatase is the most common phase for photocatalytic applications, followed by the rutile phase; the anatase phase exhibits lower absorption of solar light than the rutile phase, because the band gap of anatase is greater (3.2 eV) than that of the rutile phase (3.0 eV) [21,22]. However, synergy between these two phases results in higher photocatalytic efficiency for TiO_2, and the most efficient photocatalyst, Degussa TiO_2 powder P25, has a rutile–anatase ratio of 1:3; however, the efficiency of these phases requires efficient charge separation when the TiO_2 is irradiated. This efficiency has been associated with the migration of photoexcited electrons from the rutile phase to the conduction band of the anatase phase, while the photoexcited holes are left in the rutile phase [22–24]. The last crystalline phase, brookite, is the most difficult to synthesize due to its orthorhombic structure, which makes it more unstable than the other two phases [25,26]. The band gap reported for the brookite phase ranges from 3.1 to 3.4 eV, even though there are reports in which the band gap of this phase is 3.6 eV; therefore, the differences in the band gaps could be useful in photocatalytic processes [27–29].

Preparing a single TiO_2 phase is not easy, as the anatase phase changes to the rutile phase at approximately 600 °C, while brookite is converted into the rutile phase at approximately 800 °C [25,30]. However, as the three phases are used in photocatalytic processes, the percentages of the phases could determine the efficiency of each process. In this sense, an efficient way to use TiO_2 for heavy metal absorption is to support it on a substrate, which allows recovery and reuse. Among the methods used for depositing materials, physical techniques allow modification of the structural properties of the materials in a controlled way by changing the initial deposition conditions. Deposition of thin films via sputtering is a great option for modifying the structural properties of semiconductors, and it is possible to explore the depositional conditions to change the final properties of the film. With the sputtering technique, changing the amount of carrier gas inside the chamber, the gases used in the deposit, the power density, and the working pressure for deposition is feasible [31–34]. Among these parameters, the working pressure is one of the best options for modifying the structural, optical, and morphological properties of thin films, as the ionization levels of the species inside the chamber increase with increasing working pressures [35,36]. The working pressure affects the path and energy through which the material species collide with the substrate inside the chamber, giving rise to preferential planes in the crystalline structure [35,37–39]. However, the presence of more than two TiO_2 phases is very common even with changes in the deposition conditions (see Table S2) [32–34,40–49].

For this reason, this work explores the influence of the working pressure on the deposition of TiO_2 thin films by the sputtering technique and the efficiency for adsorbing heavy metals such as Cr(VI) and Fe(III). The structural, optical, and morphological properties were studied to understand the effects of the working pressure during deposition.

2. Experimental

2.1. Deposition of TiO_2 thin films by magnetron sputtering

TiO_2 films were deposited using a Ti target (99.995% pure, 2.0000 diameter X 0.12500 thick, Kurt J. Lesker) over glass substrates. With a turbomolecular pump, the sputtering chamber was evacuated to a background pressure of $1.14\,x\,10^{-3}$ Pa, and then Ar gas (UHP) was introduced into the chamber with a flow rate of 15 sccm. The films were deposited using a current DC power (60 W) for 60 min. Each film has been deposited at different working pressures, such as 0.47, 1.27, 2.13, and 3.47 Pa, to obtain the different TiO_2 phases. The working pressures were chosen according to the equipment conditions. After deposition, the films were annealed at 400 °C for 60 min to form the oxide.

2.2. Physicochemical characterization of TiO_2 thin films

Structural, optical, and photocatalytic properties films were characterized by X -ray diffraction (PANalytical, radiation of 1.54 Å - Cu Ka, grazing angle), UV–Vis–NIR spectrophotometer (Cary 5000, range 200–800 nm), Surface morphology was studied by atomic force microscope (ASYLUM RESEARCH, model MFP3D-SA, in Tapping mode). X-ray photoelectron spectroscopy was used to determine chemical states and elemental composition (Thermo Scientific, Escalab 250Xi, equipped with an Al Ka monochromatic X-ray source, hv = 1486.7 eV).

2.3. Photocatalytic adsorption test

The photocatalytic test was performed using the TiO_2 films as photocatalytic reactors. The adsorption of metal ions was obtained by doing a calibration using five different concentrations of Cr and Fe. The calibration plots, the absorbance of each spectrum and the equation that describes the relation between the absorbance and the metal ion concentration are shown in the Supporting Information (Fig. S1). For the photocatalytic tests, in each reactor, 30 ml of a 2-ppm solution of Cr (VI) and Fe (III) are placed and are constantly stirring at room temperature. After 30 min, the sample reference was taken, and the reactor began to be irradiated with a commercial lamp of 90 Watts (Tecnolite/HEL-BLB). The tests were performed for 360 min and were monitored using a UV–Vis–NIR spectrophotometer. The results of these tests are presented in the supplementary information (Fig. S1).

3. Results and discussion

Fig. 1a shows the X-ray diffraction patterns of the TiO_2 films. The different diffraction patterns for each film indicate that the working pressure affected the crystalline structures. This was true for films deposited at the highest (3.47 Pa) and lowest (0.47 Pa) working pressures, which showed peaks at different 2θ positions. In contrast, the films obtained at pressures of 1.27 and 2.13 Pa had amorphous structures, which are common in sputtering deposits over glass substrates [32,42,49,50]. For this reason, a Rietveld refinement was performed to determine the lattice parameters and the phases resulting from the deposition conditions (Table S3). After the Rietveld refinement, the TiO_2-0.47 film showed rutile (tetragonal) and brookite (orthorhombic) phases. However, the brookite phase was no longer formed as the working pressure was increased (from 0.47 Pa to 2.13 Pa), and the TiO_2-1.27 and TiO_2-2.13 films had mixtures of the anatase and rutile tetragonal phases. In contrast, the three TiO_2 phases, anatase, rutile, and brookite, were present only in the TiO_2-3.47 film deposited at a high working pressure (3.47 Pa). The presence of the different TiO_2 phases and changes in the lattice parameters of each film are shown in the Supporting Information (Tables S3 and S4).

To complement the XRD measurements, Raman spectroscopy was used to determine the TiO_2 structure, and the Raman spectra of the TiO_2 films are shown in Fig. 1b. All the films exhibited the vibration modes of the anatase (E_g, A_{1g}, B_{1g}, E_u, and E_{3g}), rutile (A_{1g}, E_u, and E_{3u}), and brookite (A_{1g} and B_{2g}) phases. For the anatase phase, the principal vibrational modes (E_g, A_{1g}, B_{1g}) were those involving oscillations of the O atoms in O–Ti–O, O_2 pure vibrations, and Ti atom vibrations [51,52]. The A_{1g} and E_{3u} modes for the rutile phase involved atomic displacements of the oxygen sublattice and the IR-active polar modes, respectively [52,53]. Likewise, the A_{1g} and B_{2g} modes of the brookite phase have been used to identify this TiO_2 phase [54,55].

The transmittance percentages of the TiO_2 films are presented in Fig. 2a. As the pressure increased (from 1.27 Pa to 3.47 Pa), the transmittances increased to between 70 and 90%, except for the TiO_2-0.47 film (deposited at lower pressure 0.47 Pa), for which the transmittance was less than 5%. The optical band gap was calculated from the Tauc plot by extrapolating the linear portion, where α is the absorption coefficient, $h\nu$ is the photon energy and E_g is the optical band gap energy (Fig. S2) [7]. As the pressure increased (from 0.47 Pa to 3.47 Pa), the band gap values were 3.74, 3.54, 3.32, and 3.6 eV for the TiO_2-0.47, TiO_2-1.27, TiO_2-2.13, and TiO_2-3.47 films, respectively. These values were consistent with the band gaps of the different TiO_2 phases [21,56]. The transmittance spectra showed that the adsorption edges of the films were shifted to higher wavelengths, and the bandgaps increased in the order TiO_2-2.13, TiO_2-3.47, and TiO_2-1.27. These shifts raised the Fermi levels above the conduction band and increased the band gaps [57]. This behavior is known as the Burstein–Moss effect, and it can be caused by dopants or structural defects that increase the concentrations of carriers and modify the absorption edge [57]. Optical properties such as ellipsometry angles, refractive index and PL spectra are shown in Figs. S3 and S4 (Supporting Information) [58,59].

The surfaces of the films were analyzed with atomic force microscopy (AFM) over a 1.0 × 1.0 μm area. Fig. 2b shows that all films had the same grain morphologies because the grain sizes varied according to the working pressure used for deposition. The RMS,

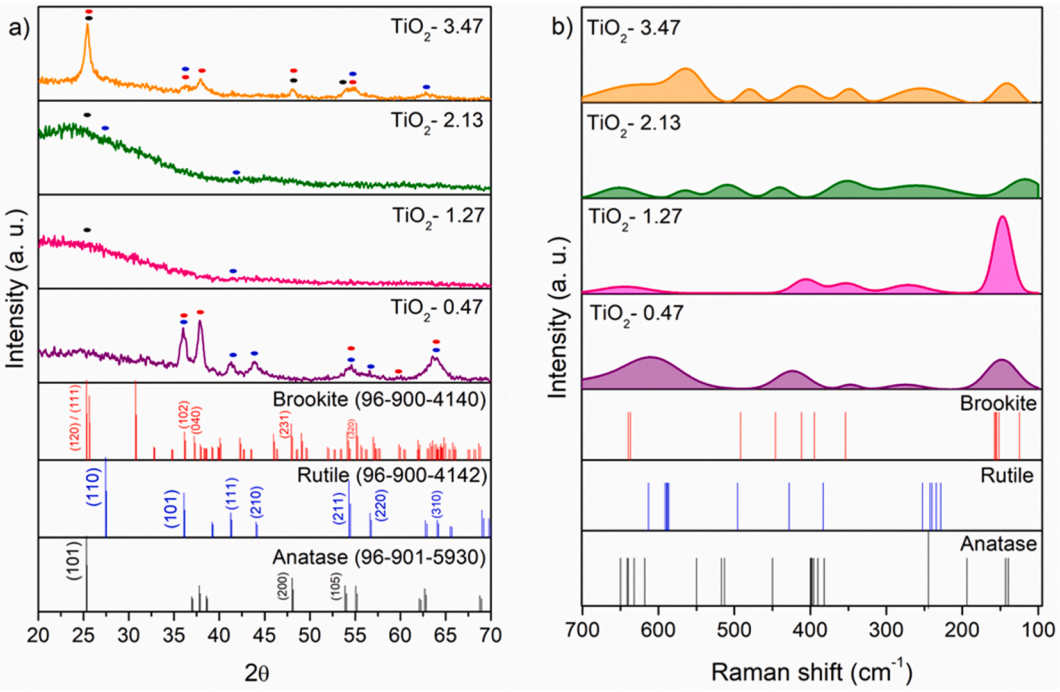

Fig. 1. a) XRD patterns and b) Raman spectra of the TiO_2 films deposited at different working pressures. The black, blue, and red dots in the XRD patterns correspond to the anatase, rutile, and brookite phases, respectively. (For interpretation of the references to color in this figure legend, the reader is referred to the Web version of this article.)

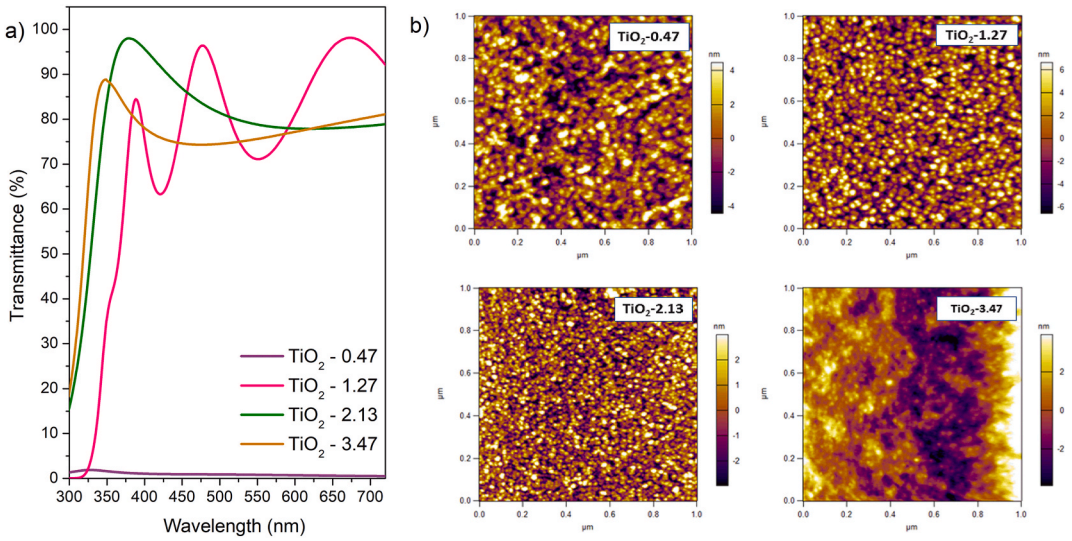

Fig. 2. a) Transmittance spectra and b) AFM images of the TiO_2 films deposited at different working pressures.

average height, and specific surface area were measured with AFM, and the values were 3.01, 3.12, 1.46, and 1.97 nm for the roughness; 7.68, 11.10, 4.93, and 5.93 nm for the average height; and approximately 1 nm^2 for the surface areas of TiO_2-0.47, TiO_2-1.27, TiO_2-2.13, and TiO_2-3.47, respectively.

The importance of surface defects in the photocatalytic performance of TiO_2 has already been identified, especially for CO_2 photocatalytic reduction [51,60]. In particular, oxygen vacancies serve as adsorption and active sites in heterogeneous photocatalysis and modify the electronic structure, charge transport, and surface properties [61,62]. For this reason, XPS was used to determine the oxidation states of titanium and the concentration of oxygen vacancies. High-resolution Ti 2p and O 1s spectra were fitted with a Shirley background. A comparison among the four samples is shown in Fig. 3. Different authors have claimed that the titanium in TiO_2 crystals exhibited both the 3^+ and 4^+ oxidation states [60]. However, in the Ti 2p spectra, only a doublet peak at 458.4 eV with a spin-orbital splitting of 5.7 eV was identified. This peak was attributed to Ti^{4+} bonded to O^{2-} [63]. The peak located at a higher binding energy (471.8 eV) was identified as a satellite peak. On the other hand, the O 1s spectrum contained five peaks. The peaks at

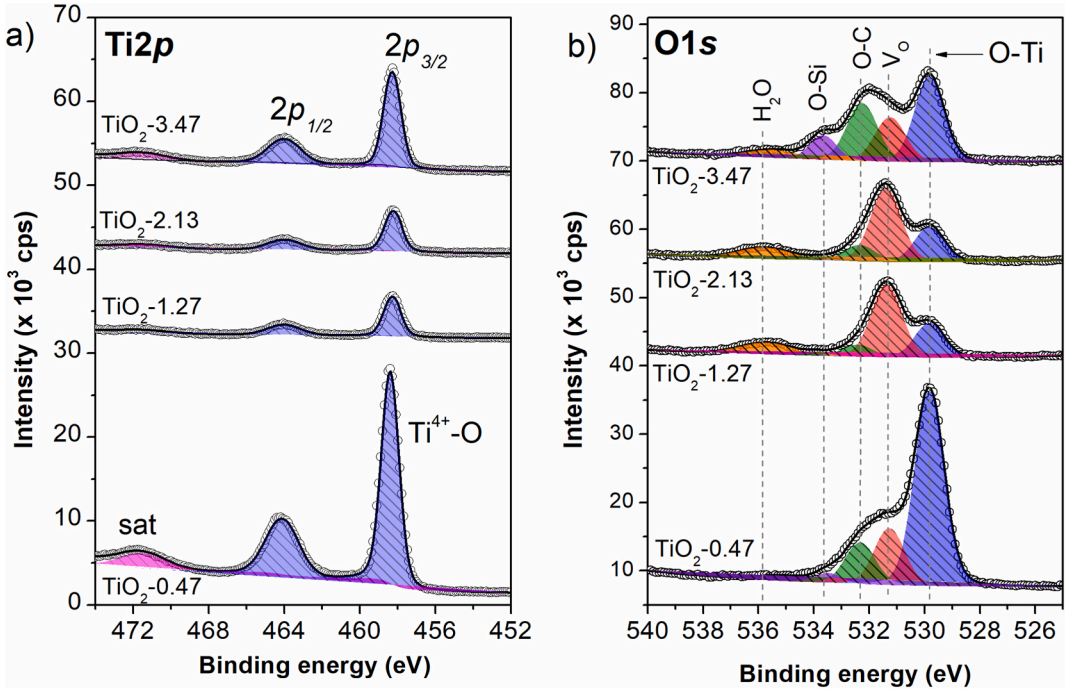

Fig. 3. High-resolution spectra for a) Ti 2p and b) O 1s core levels for TiO_2 films deposited at different working pressures.

529.8, 530.8, 531.5, 532.4 and 533.7 eV were attributed to $O^{2-}Ti^{4+}$ species in TiO_2, oxygen vacancies, chemisorbed species (hydroxyl groups), -*O*-C=O bonds and oxygen bonded to silicon, respectively [63–66]. A small peak at 103.2 eV (Si–O bonds) was seen in the survey spectra of the TiO_2-0.47 and TiO_2-3.47 samples, which confirmed the peaks found in the oxygen spectrum [67].

The Ti 2p and O 1s peak intensities and their appropriate atomic sensitivity factors (ASFs) (obtained from the Scofield table) were used to determine the surface atomic compositions of the TiO_2 samples. The atomic percentages indicated by XPS for the TiO_2-0.47 and TiO_2-3.47 samples are shown in Table 1. A quantitative analysis indicated that the oxygen vacancy concentrations were highest in the TiO_2-1.27 and TiO_2-2.13 samples, which could be associated with better photocatalytic performance.

Photocatalytic adsorption of the different samples are shown in the supplementary material(Figure S5, S6 and S7), and based on these results, we focused on the films that showed higher capacities for the adsorption of Cr (VI) and Fe (III) ions. Hence, the amounts of Cr^{6+} and Fe^{3+} ions adsorbed on the surfaces were determined for the TiO_2-0.47 and TiO_2-2.13 films, respectively. The relationship between the removal efficiency for a given interaction time and the adsorption capacity (q_t) of TiO_2 is shown in Fig. 4. The iron plot exhibited a constant linear trend over time, which provided information on the homogeneity of the films and the reactive sites at the surface. On the other hand, the chromium plot shows three levels, suggesting that physisorption had occurred; the first layer (ions physically bonded) was removed, followed by chemisorption at the surface. The different adsorption capacities for the two ions were related to the chemical nature of the solution. The sizes of the ions could have caused rearrangement at the surface and led to the adsorption of more Cr^{6+} (with the smaller radius: 58 p.m.) than Fe^{3+} (63 p.m.). Moreover, Cr^{6+} is more electropositive than Fe^{3+}, which means that it is strongly attracted to negative species such as oxygen. The percentages of Cr(VI) and Fe(III) removal were 70 and 63%, respectively, after 360 min. These values were consistent with those reported in the literature for these ions [68–70].

The absorption capacities for the films with each metal were different because heavy metals have high affinities for hydroxyl (OH^-) ions [9,10]. Therefore, the presence of hydroxyls on a film surface increases the likelihood of adsorbing metals. Based on the XPS (Table 1) results, the TiO_2-2.13 film had a higher concentration of OH^- species on the surface, which increased the amount of Fe^{3+} adsorbed. In contrast, the TiO_2-0.47 film, with a major brookite component, did not have a high concentration of OH^- ions. However, as mentioned above, Cr^{6+} is an electropositive metal with a strong attraction for negative species such as oxygen, and the XPS results indicated that the TiO_2-0.47 film had a lower oxygen deficiency, which favored Cr^{6+} adsorption.

To confirm the presence of these ions on the surfaces of the TiO_2 thin films, TiO_2-0.47 and TiO_2-2.13 were analyzed via EDS and UV–Vis spectroscopy. Fig. 5 shows the SEM−EDS maps of the 0.47-TiO_2-Cr (top) and 2.13-TiO_2-Fe (bottom) samples, with the different distribution of elements O, Ti and Fe/Cr obtained by EDS measurements (around 1–2 μm in depth). The colored elemental maps showed that O (red), Ti (blue), and Cr or Fe (green) were homogeneously distributed throughout the entire thin film. The atomic composition of the TiO_2 samples with Cr was O 60.4%, Ti 36.3%, and Cr 3.3%, while that with Fe was O 65.0%, Ti 33.8%, and Fe 1.2%. These results showed that the concentration of Cr in the TiO_2 was greater than that of Fe after 350 min of UV exposure, consistent with the adsorption capacities. Moreover, the UV–Vis spectra revealed decreased transmittance after adsorption of the metals, suggesting the formation of a thin layer of species at the surface. A decrease was also observed even for the TiO_2-0.47 sample, which exhibited approximately 2% transmittance at 300–500 nm, or approximately zero. These measurements indirectly confirmed the adsorption of species on the surfaces.

4. Conclusions

TiO_2 thin films were deposited on glass substrates via magnetron sputtering to study the impact of the working pressure on the physicochemical properties. Combinations of the anatase, rutile and brookite phases were obtained by modifying the working pressures. XRD and Raman spectrometry revealed that the TiO_2-0.47 and TiO_2-3.47 samples were composed of brookite, rutile and anatase, while the TiO_2-1.27 and TiO_2-2.13 samples comprised anatase and rutile mixture. In the same way, the films deposited at higher pressures (1.27, 2.13, and 3.47 Pa) have the highest transmittance percentage (>70%), while the film deposit at 0.47 Pa has a transmittance percentage lower than 5%. Meanwhile, in AFM, results observed that the surface of the films was composed of little grains that agglomerated as the working pressure increased in each deposit (from 0.47 to 3.47 Pa). On the other hand, XPS results show that the principal contribution in the TiO_2 films is the Ti^{4+} bonded to O^{2+} species, as well as oxygen vacancies, chemisorbed species, and O–C=O bonds. According to the photocatalytic results, the TiO_2 samples preferably adsorbed Cr (VI) over Fe (III) and exhibited maximum adsorption capacities ranging from 53 to 334.5 mg/g for Cr (VI) and from 149.8 to 271.3 mg/g for Fe (III) ions in aqueous solutions, as shown with batch adsorption experiments. The higher adsorption capacity for Cr was presumably due to the small ionic radius, the electropositive nature of this element and the roughness of the TiO_2 thin film. The charge affinity and the metal electronegativity influenced the absorption capacity of each film, as Fe^{2+} adsorption depended on hydroxyl (OH^-) species, and the presence of more oxygen increased the amounts of the electronegative metals adsorbed, as seen with Cr^{6+}. After each reaction, the transmittance percentage and SEM-EDS measurements were done to confirm the presence of the metals over the film surface. SEM−EDS maps of each

Table 1
Atomic percentage of titanium and oxygen species in the TiO_2 thin films calculated from XPS spectra.

Sample	Ti 2*p* (Ti–O)	O 1*s* (O–Ti)	O 1*s* (Vo)	O 1*s* (OH^-)	O 1*s* (O–C)	O 1*s* (O–Si)
M1	22.5	48.5	4.9	11.9	9.7	2.5
M2	11.5	22.5	14.0	42.9	9.2	0.0
M3	11.3	21.5	13.5	41.4	12.3	0.0
M4	15.2	32.5	7.9	14.9	20.3	9.3

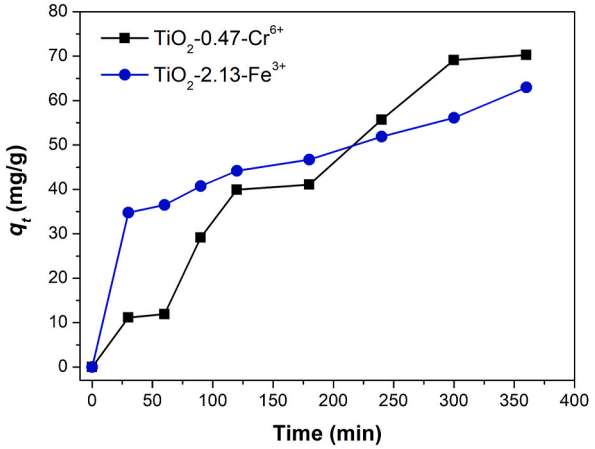

Fig. 4. Adsorption kinetics of TiO_2 samples adsorbing Cr and Fe in aqueous solution.

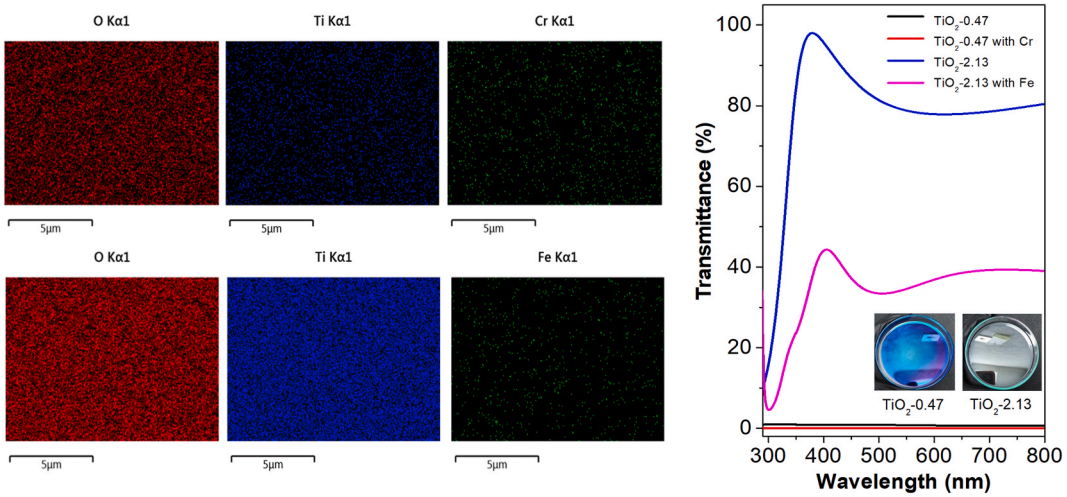

Fig. 5. Scanning SEM-EDS mapping of TiO_2 thin films after adsorption of Cr (top) and Fe (bottom) and transmittance spectra for these samples.

film, revealed the presence of Cr and Fe at the surface, with contents of 3.3 and 1.2%, respectively. In contrast, the transmittance percentage of all films decreased, which confirmed the presence of the different metals over the film surface and the capacity of TiO2 to absorb different metals.

Data availability statement

The data will be available on request.

CRediT authorship contribution statement

F.A. Hernández-Rodríguez: Writing – original draft, Methodology, Investigation. **R. Garza-Hernández:** Writing – review & editing, Writing – original draft, Investigation, Formal analysis. **M.R. Alfaro-Cruz:** Writing – review & editing, Writing – original draft, Supervision, Investigation, Formal analysis, Conceptualization. **Leticia M. Torres-Martínez:** Writing – review & editing, Supervision, Resources, Funding acquisition.

Declaration of competing interest

The authors declare that they have no known competing financial interests or personal relationships that could have appeared to influence the work reported in this paper.

Acknowledgments

The authors would like to thank CONAHCYT for the scholarship support of F.A. Hernández-Rodríguez (CVU 1150215), and for the support to the following projects: Investigadores e Investigadoras por México-CONAHCYT 363, and Paradigmas y Fronteras de la Ciencia 320379; and UANLfor PAYCIT projects CE1771-21, 277-CE-2022. We also thanks Dr. Oscar Ceballos Sánchez (CUCEI-UDG), Andrés Isaak González Jacquez, Alejandro Arizpe and Oscar Vega (CIMAV) for his technical support in the XPS, XRD and AFM measurements. We also appreciate the facilities of Dr. Ismael Flores Vivian and Iris Alessandra Alanis Leal, CIMAC UANL for their technical support in the SEM measurements.

Appendix A. Supplementary data

Supplementary data to this article can be found online at https://doi.org/10.1016/j.heliyon.2024.e27359.

References

[1] S. Kanan, M.A. Moyet, R.B. Arthur, H.H. Patterson, Recent advances on TiO_2-based photocatalysts toward the degradation of pesticides and major organic pollutants from water bodies, Catal. Rev. - Sci. Eng. 62 (2020) 1–65, https://doi.org/10.1080/01614940.2019.1613323.
[2] X. Chen, S.S. Mao, Titanium dioxide nanomaterials: synthesis, properties, modifications and applications, Chem. Rev. 107 (2007) 2891–2959, https://doi.org/10.1021/cr0500535.
[3] H.N.C. Dharma, J. Jaafar, N. Widiastuti, H. Matsuyama, S. Rajabsadeh, M.H.D. Othman, M.A. Rahman, N.N.M. Jafri, N.S. Suhaimin, A.M. Nasir, N.H. Alias, A review of titanium dioxide (TiO2)-based photocatalyst for oilfield-produced water treatment, Membranes 12 (2022), https://doi.org/10.3390/membranes12030345.
[4] R. Kumar Patnaik, N. Divya, A brief review on the synthesis of TiO_2 thin films and its application in dye degradation, Mater. Today Proc. 72 (2023) 2749–2756, https://doi.org/10.1016/j.matpr.2022.10.064.
[5] N. Madima, K.K. Kefeni, S.B. Mishra, A.K. Mishra, TiO_2-modified g-C_3N_4 nanocomposite for photocatalytic degradation of organic dyes in aqueous solution, Heliyon 8 9 (2022) e10683, https://doi.org/10.1016/j.heliyon.2022.e10683.
[6] D. Komaraiah, P. Madhukar, Y. Vijayakumar, M.V. Ramana Reddy, R. Sayanna, Photocatalytic degradation study of methylene blue by brookite TiO_2 thin film under visible light irradiation, Mater, Today Proc 3 (2016) 3770–3778, https://doi.org/10.1016/j.matpr.2016.11.026.
[7] M.R. Alfaro Cruz, D. Sanchez-Martinez, L.M. Torres-Martínez, Optical properties of TiO_2 thin films deposited by DC sputtering and their photocatalytic performance in photoinduced process, Int. J. Hydrogen Energy 44 (2019) 20017–20028, https://doi.org/10.1016/j.ijhydene.2019.06.043.
[8] M.R. Alfaro Cruz, D. Sanchez-Martinez, L.M. Torres-Martínez, TiO_2 nanorods grown by hydrothermal method and their photocatalytic activity for hydrogen production, Mater. Lett. 237 (2019) 310–313, https://doi.org/10.1016/j.matlet.2018.11.040.
[9] Z. Raji, A. Karim, A. Karam, S. Khalloufi, Adsorption of heavy metals: mechanisms, kinetics, and applications of various adsorbents in wastewater remediation—a review, Waste 1 (2023) 775–805, https://doi.org/10.3390/waste1030046.
[10] N.A.A. Qasem, R.H. Mohammed, D.U. Lawal, Removal of heavy metal ions from wastewater: a comprehensive and critical review, Npj Clean Water 4 (2021), https://doi.org/10.1038/s41545-021-00127-0.
[11] M. Sharma, J. Singh, S. Hazra, S. Basu, Adsorption of heavy metal ions by mesoporous ZnO and TiO_2@ZnO monoliths: adsorption and kinetic studies, Microchem. J. 145 (2019) 105–112, https://doi.org/10.1016/j.microc.2018.10.026.
[12] C. Wang, Y. Zhan, Y. Wu, X. Shi, Y. Du, Y. Luo, H. Deng, TiO_2/rectorite-trapped cellulose composite nanofibrous mats for multiple heavy metal adsorption, Int. J. Biol. Macromol. 183 (2021) 245–253, https://doi.org/10.1016/j.ijbiomac.2021.04.085.
[13] P. Xuchao, H. Yong, D.T. Semirumi, F. Zhong, R. Rezaie, Development of cellulose/hydroxyapatite/TiO_2 scaffolds for efficient removal of lead (II) ions pollution: characterization, kinetic analysis, and artificial neural network modeling, Int. J. Biol. Macromol. 246 (2023) 125630, https://doi.org/10.1016/j.ijbiomac.2023.125630.
[14] A. Maleki, B. Hayati, F. Najafi, F. Gharibi, S.W. Joo, Heavy metal adsorption from industrial wastewater by PAMAM/TiO_2 nanohybrid: preparation, characterization and adsorption studies, J. Mol. Liq. 224 (2016) 95–104, https://doi.org/10.1016/j.molliq.2016.09.060.
[15] W. Wang, S. Zhu, N. Li, S. Xie, C. Wen, X. Luo, Enhanced Cd^{2+} adsorption and toxicity for microbial biofilms in the presence of TiO_2 nanoparticles, Environ. Pollut. 314 (2022) 120239, https://doi.org/10.1016/j.envpol.2022.120239.
[16] A.B. Đukić, K.R. Kumrić, N.S. Vukelić, Z.S. Stojanović, M.D. Stojmenović, S.S. Milošević, L.L. Matović, Influence of ageing of milled clay and its composite with TiO_2 on the heavy metal adsorption characteristics, Ceram. Int. 41 (2015) 5129–5137, https://doi.org/10.1016/j.ceramint.2014.12.085.
[17] N.G. Mostafa, A.F. Yunnus, A. Elawwad, Adsorption of Pb(II) from water onto ZnO, TiO_2, and Al_2O_3: process study, adsorption behaviour, and thermodynamics, Adsorpt. Sci. Technol. 2022 (2022), https://doi.org/10.1155/2022/7582756.
[18] Y. Yang, G. Wang, Q. Deng, H. Wang, Y. Zhang, D.H.L. Ng, H. Zhao, Enhanced photocatalytic activity of hierarchical structure TiO_2 hollow spheres with reactive (001) facets for the removal of toxic heavy metal Cr(vi), RSC Adv. 4 (2014) 34577–34583, https://doi.org/10.1039/c4ra04787g.
[19] D. Kanakaraju, M.A. Bin Abdullah, L.Y. Chin, TiO_2/PKSAC functionalized with Fe_3O_4 for efficient concurrent removal of heavy metal ions from water, Colloids Interface Sci. Commun. 40 (2021) 100353, https://doi.org/10.1016/j.colcom.2020.100353.
[20] R. Zha, R. Nadimicherla, X. Guo, Cadmium removal in waste water by nanostructured TiO_2 particles, J. Mater. Chem. A 2 (2014) 13932–13941, https://doi.org/10.1039/c4ta02106a.
[21] J. Zhang, P. Zhou, J. Liu, J. Yu, New understanding of the difference of photocatalytic activity among anatase, rutile and brookite TiO_2, Phys. Chem. Chem. Phys. 16 (2014) 20382–20386, https://doi.org/10.1039/c4cp02201g.
[22] G. Zerjav, K. Zizek, J. Zavasnik, A. Pintar, Brookite vs. rutile vs. anatase: what's behind their various photocatalytic activities? J. Environ. Chem. Eng. 10 (2022) https://doi.org/10.1016/j.jece.2022.107722.
[23] Y.K. Kho, A. Iwase, W.Y. Teoh, L. Mädler, A. Kudo, R. Amal, Photocatalytic H_2 evolution over TiO_2 nanoparticles. The synergistic effect of anatase and rutile, J. Phys. Chem. C 114 (2010) 2821–2829, https://doi.org/10.1021/jp910810r.
[24] B. Ohtani, O.O. Prieto-Mahaney, D. Li, R. Abe, What is Degussa (Evonic) P25? Crystalline composition analysis, reconstruction from isolated pure particles and photocatalytic activity test, J. Photochem. Photobiol. Chem. 216 (2010) 179–182, https://doi.org/10.1016/j.jphotochem.2010.07.024.
[25] L.E. Oi, M.Y. Choo, H.V. Lee, H.C. Ong, S.B.A. Hamid, J.C. Juan, Recent advances of titanium dioxide (TiO_2) for green organic synthesis, RSC Adv. 6 (2016) 108741–108754, https://doi.org/10.1039/c6ra22894a.
[26] S. Cao, N. Sui, P. Zhang, T. Zhou, J. Tu, T. Zhang, TiO_2 nanostructures with different crystal phases for sensitive acetone gas sensors, J. Colloid Interface Sci. 607 (2022) 357–366, https://doi.org/10.1016/j.jcis.2021.08.215.
[27] M. Landmann, E. Rauls, W.G. Schmidt, The electronic structure and optical response of rutile, anatase and brookite TiO_2, J. Phys. Condens. Matter 24 (2012), https://doi.org/10.1088/0953-8984/24/19/195503.

[28] H. Lin, L. Li, M. Zhao, X. Huang, X. Chen, G. Li, R. Yu, Synthesis of high-quality brookite TiO_2 single-crystalline nanosheets with specific facets exposed: tuning catalysts from inert to highly reactive, J. Am. Chem. Soc. 134 (2012) 8328–8331, https://doi.org/10.1021/ja3014049.

[29] A. Di Paola, M. Bellardita, L. Palmisano, Brookite, the Least Known TiO_2 Photocatalyst, 2013, https://doi.org/10.3390/catal3010036.

[30] M. Manzoli, F.S. Freyria, N. Blangetti, B. Bonelli, Brookite, a sometimes under evaluated TiO_2 polymorph, RSC Adv. 12 (2022) 3322–3334, https://doi.org/10.1039/d1ra09057g.

[31] M. Pérez-González, M. Morales-Luna, J. Santoyo-Salazar, H. Crotte-Ledesma, P.E. García-Tinoco, S.A. Tomás, Improved adsorption and photocatalytic removal of methylene blue by MoO_3 thin films: role of the sputtering power, film thickness, and sputtering working pressure, Catal. Today 360 (2021) 138–146, https://doi.org/10.1016/j.cattod.2019.06.003.

[32] S.S. Kamble, J.K. Radhakrishnan, Influence of O_2 flow rate on the characteristics of TiO_2 thin films deposited by RF reactive sputtering, Mater. Today Proc. 45 (2021) 3915–3919, https://doi.org/10.1016/j.matpr.2020.07.405.

[33] A. Kozlovskiy, I. Shlimas, K. Dukenbayev, M. Zdorovets, Structure and corrosion properties of thin TiO_2 films obtained by magnetron sputtering, Vacuum 164 (2019) 224–232, https://doi.org/10.1016/j.vacuum.2019.03.026.

[34] S. Gürakar, H. Ot, S. Horzum, T. Serin, Variation of structural and optical properties of TiO_2 films prepared by DC magnetron sputtering method with annealing temperature, Mater. Sci. Eng. B 262 (2020) 114782, https://doi.org/10.1016/j.mseb.2020.114782.

[35] K. Seshan, Handbook of Thin-Film Deposition Processes and Techniques, second ed., William Andrew Publishing, Norwich, New York, U.S.A., 2002.

[36] M.J. Zhao, J.F. Zhang, Q.H. Huang, W.Y. Wu, M.C. Tseng, S.Y. Lien, W.Z. Zhu, Effect of working pressure on Sn/In composition and optoelectronic properties of ITO films prepared by high power impulse magnetron sputtering, Vacuum 196 (2022) 110762, https://doi.org/10.1016/j.vacuum.2021.110762.

[37] S.I. Son, D. Shin, Y.G. Son, C.S. Son, D.R. Kim, J.H. Park, S. Kim, D. Hwang, P. Song, Effect of working pressure on the properties of RF sputtered SnS thin films and photovoltaic performance of SnS-based solar cells, J. Alloys Compd. 831 (2020) 154626, https://doi.org/10.1016/j.jallcom.2020.154626.

[38] H. Kong, J. He, L. Huang, L. Zhu, L. Sun, P. Yang, J. Chu, Effect of working pressure on growth of Cu(In,Ga)Se_2 thin film deposited by sputtering from a single quaternary target, Mater. Lett. 116 (2014) 75–78, https://doi.org/10.1016/j.matlet.2013.10.112.

[39] V.K. Arepalli, Y. Shin, J. Kim, Influence of working pressure on the structural, optical, and electrical properties of RF-sputtered SnS thin films, Superlattice. Microst. 122 (2018) 253–261, https://doi.org/10.1016/j.spmi.2018.08.001.

[40] J. Daughtry, A.S. Alotabi, L. Howard-Fabretto, G.G. Andersson, Composition and properties of RF-sputter deposited titanium dioxide thin films, Nanoscale Adv. 3 (2021) 1077–1086, https://doi.org/10.1039/d0na00861c.

[41] A. Panepinto, M. Michiels, M.T. Dürrschnabel, L. Molina-Luna, C. Bittencourt, P.A. Cormier, R. Snyders, Synthesis of anatase (Core)/Rutile (shell) nanostructured TiO_2 thin films by magnetron sputtering methods for dye-sensitized solar cell applications, ACS Appl. Energy Mater. 3 (2020) 759–767, https://doi.org/10.1021/acsaem.9b01910.

[42] A. Sezgin, R. Čtvrtlík, L. Václavek, J. Tomáštík, L. Nožka, E. Menşur, S. Türküz, Optical, structural and mechanical properties of TiO_2 and TiO_2-ZrO_2 thin films deposited on glass using magnetron sputtering, Mater. Today Commun. 35 (2023), https://doi.org/10.1016/j.mtcomm.2023.106334.

[43] H. Kikuchi, M. Kitano, M. Takeuchi, M. Matsuoka, M. Anpo, P.V. Kamat, Extending the photoresponse of TiO_2 to the visible light region: photoelectrochemical behavior of TiO_2 thin films prepared by the radio frequency magnetron sputtering deposition method, J. Phys. Chem. B 110 (2006) 5537–5541, https://doi.org/10.1021/jp058262g.

[44] J.Y. Zheng, S.H. Bao, Y. Guo, P. Jin, Anatase TiO_2 films with dominant {001} facets fabricated by direct-current reactive magnetron sputtering at room temperature: oxygen defects and enhanced visible-light photocatalytic behaviors, ACS Appl. Mater. Interfaces 6 (2014) 5940–5946, https://doi.org/10.1021/am500979j.

[45] B.I. Stefanov, G.A. Niklasson, C.G. Granqvist, L. Österlund, Quantitative relation between photocatalytic activity and degree of ⟨001⟩ orientation for anatase TiO_2 thin films, J. Mater. Chem. A 3 (2015) 17369–17375, https://doi.org/10.1039/c5ta04362j.

[46] D. Rafieian, R.T. Driessen, W. Ogieglo, R.G.H. Lammertink, Intrinsic photocatalytic assessment of reactively sputtered TiO_2 films, ACS Appl. Mater. Interfaces 7 (2015) 8727–8732, https://doi.org/10.1021/acsami.5b01047.

[47] Y. Du, H. Cai, Y. Wu, Z. Xing, Z. Li, J. Xu, L. Huang, J. Ni, J. Li, J. Zhang, Enhanced planar perovskite solar cells with efficiency exceeding 16% via reducing the oxygen vacancy defect state in titanium oxide electrode, Phys. Chem. Chem. Phys. 19 (2017) 13679–13686, https://doi.org/10.1039/c7cp01936j.

[48] G.J. Choi, H. Jung, D.H. Kim, Y. Sohn, J.S. Gwag, Photoelectrocatalytic effect of unbalanced RF magnetron sputtered TiO2 thin film on ITO-coated patterned SiO_2 nanocone arrays, Catal. Sci. Technol. 8 (2018) 898–906, https://doi.org/10.1039/c7cy02371e.

[49] S.H. Salman, A.A. Shihab, A.H.K. Elttayef, Studying the effect of the type of substrate on the structural ,morphology and optical properties of TiO_2 thin films prepared by RF magnetron sputtering, Energy Proc. 157 (2019) 199–207, https://doi.org/10.1016/j.egypro.2018.11.181.

[50] A.S. Alkadem Idriss, N.N.A. Nik Ab Razak, N.M. Ahmed, Y.A. Abdulla, Thermoluminescence properties of TiO_2/Cu/TiO_2 multilayer thin films fabricated by (RF/DC) sputtering for radiation dosimetry, J. Lumin. 260 (2023) 119886, https://doi.org/10.1016/j.jlumin.2023.119886.

[51] H. Zhao, F. Pan, Y. Li, A review on the effects of TiO_2 surface point defects on CO_2 photoreduction with H2O, J. Mater. 3 (2017) 17–32, https://doi.org/10.1016/j.jmat.2016.12.001.

[52] O. Frank, M. Zukalova, B. Laskova, J. Kürti, J. Koltai, L. Kavan, Raman spectra of titanium dioxide (anatase, rutile) with identified oxygen isotopes (16, 17, 18), Phys. Chem. Chem. Phys. 14 (2012) 14567–14572, https://doi.org/10.1039/c2cp42763j.

[53] D.K. Takci, Synthesis, characterization and dielectric properties of rutile TiO_2 nanoflowers, J. Cryst. Growth 578 (2022), https://doi.org/10.1016/j.jcrysgro.2021.126442.

[54] M.C. Ceballos-Chuc, C.M. Ramos-Castillo, J.J. Alvarado-Gil, G. Oskam, G. Rodríguez-Gattorno, Influence of brookite impurities on the Raman spectrum of TiO_2 anatase nanocrystals, J. Phys. Chem. C 122 (2018) 19921–19930, https://doi.org/10.1021/acs.jpcc.8b04987.

[55] H.H. Do, T.K.C. Tran, T.D.T. Ung, N.T. Dao, D.D. Nguyen, T.H. Trinh, T.D. Hoang, T.L. Le, T.T.H. Tran, Controllable fabrication of photocatalytic TiO_2 brookite thin film by 3D-printing approach for dyes decomposition, J. Water Process Eng. 43 (2021) 102319, https://doi.org/10.1016/j.jwpe.2021.102319.

[56] H. Tran Thi Thuong, C. Tran Thi Kim, L. Nguyen Quang, H. Kosslick, Highly active brookite TiO_2-assisted photocatalytic degradation of dyes under the simulated solar−UVA radiation, Prog. Nat. Sci. Mater. Int. 29 (2019) 641–647, https://doi.org/10.1016/j.pnsc.2019.10.001.

[57] L. Jianguo, S. Fujita, T. Kawaharamura, H. Nishinaka, Carrier concentration dependence of band gap shift in n -type ZnO:Al films, J. Appl. Phys. 101 (2007) 083705, https://doi.org/10.1063/1.2721374.

[58] B. Liu, L. Wen, X. Zhao, The photoluminescence spectroscopic study of anatase TiO_2 prepared by magnetron sputtering, Mater. Chem. Phys. 106 (2007) 350–353, https://doi.org/10.1016/j.matchemphys.2007.06.012.

[59] N.D. Abazović, M.I. Čomor, M.D. Dramićanin, D.J. Jovanović, S.P. Ahrenkiel, J.M. Nedeljković, Photoluminescence of anatase and rutile TiO_2 particles, J. Phys. Chem. B 110 (2006) 25366–25370, https://doi.org/10.1021/jp064454f.

[60] B. Bharti, S. Kumar, H.N. Lee, R. Kumar, Formation of oxygen vacancies and Ti^{3+} state in TiO_2 thin film and enhanced optical properties by air plasma treatment, Sci. Rep. 6 (2016) 1–12, https://doi.org/10.1038/srep32355.

[61] X. Pan, M.Q. Yang, X. Fu, N. Zhang, Y.J. Xu, Defective TiO_2 with oxygen vacancies: synthesis, properties and photocatalytic applications, Nanoscale 5 (2013) 3601–3614, https://doi.org/10.1039/c3nr00476g.

[62] X. Bi, G. Du, A. Kalam, D. Sun, Y. Yu, Q. Su, B. Xu, A.G. Al-Sehemi, Tuning oxygen vacancy content in TiO_2 nanoparticles to enhance the photocatalytic performance, Chem. Eng. Sci. 234 (2021) 116440, https://doi.org/10.1016/j.ces.2021.116440.

[63] B. Erdem, R.A. Hunsicker, G.W. Simmons, E. David Sudol, V.L. Dimonie, M.S. El-Aasser, XPS and FTIR surface characterization of TiO_2 particles used in polymer encapsulation, Langmuir 17 (2001) 2664–2669, https://doi.org/10.1021/la0015213.

[64] P. Krishnan, M. Liu, P.A. Itty, Z. Liu, V. Rheinheimer, M.H. Zhang, P.J.M. Monteiro, L.E. Yu, Characterization of photocatalytic TiO_2 powder under varied environments using near ambient pressure X-ray photoelectron spectroscopy, Sci. Rep. 7 (2017) 1–11, https://doi.org/10.1038/srep43298.

[65] D. Barreca, A. Gasparotto, C. Maccato, C. Maragno, E. Tondello, TiO_2 thin films by chemical vapor deposition: an XPS characterization, Surf. Sci. Spectra 14 (2007) 27–33, https://doi.org/10.1116/11.20070902.

[66] A. Sanchez-Martinez, C. Koop-Santa, O. Ceballos-Sanchez, E.R. López-Mena, M.A. González, V. Rangel-Cobián, E. Orozco-Guareño, M. García-Guaderrama, Study of the preparation of TiO_2 powder by different synthesis methods, Mater. Res. Express 6 (2019), https://doi.org/10.1088/2053-1591/ab21e8.
[67] D.S. Jensen, S.S. Kanyal, N. Madaan, M.A. Vail, A.E. Dadson, M.H. Engelhard, M.R. Linford, Silicon (100)/SiO_2 by XPS, Surf. Sci. Spectra 20 (2013) 36–42, https://doi.org/10.1116/11.20121101.
[68] Y. Song, X. Lu, Z. Liu, W. Liu, L. Gai, X. Gao, H. Ma, Efficient removal of Cr(VI) by TiO_2 based micro-nano reactor via the synergy of adsorption and photocatalysis, Nanomaterials 12 (2022) 1–15, https://doi.org/10.3390/nano12020291.
[69] K.M. Joshi, V.S. Shrivastava, Photocatalytic degradation of Chromium (VI) from wastewater using nanomaterials like TiO_2, ZnO, and CdS, Appl. Nanosci. 1 (2011) 147–155, https://doi.org/10.1007/s13204-011-0023-2.
[70] K. Uma, S. Pawar, TiO_2/g-C_3N_4 composites for the removal of chromium in wastewater, Results Chem 5 (2023) 3–9, https://doi.org/10.1016/j.rechem.2022.100743.